Supporting Information

Bromide-induced Highly Oriented Low-Dimensional Ruddlesden–Popper Phase for Efficient and Stable Perovskite Solar Cells

Jianfei Hu,[a] Jin Liu,[a] Haoran Chen,[a] Xueqin Ran,[a] Hui Zhang,[a] Ping Li,[a] Lin Song,[b] Peter Müller-Buschbaumcd,[cd] Yingdong Xia,[*a] Yonghua Chen[a]

[a]Key Laboratory of Flexible Electronics (KLOFE) & Institution of Advanced Materials (IAM), Nanjing Tech University (NanjingTech), Nanjing 211816, Jiangsu, P. R. China.

[b]Frontiers Science Center for Flexible Electronics, Xi'an Institute of Flexible Electronics (IFE) and Xi'an Institute of Biomedical Materials & Engineering, Northwestern Polytechnical University, Xi'an 710072, P. R. China.

[c]Lehrstuhl für Funktionelle Materialien, Physik Department, Technische Universität München. James-Franck-Str. 1, 85748 Garching, Germany

[d]Heinz Maier-Leibnitz Zentrum (MLZ), Technische Universität München, Lichtenbergstr. 1, 85748 Garching, Germany

Email: iamydxia@njtech.edu.cn

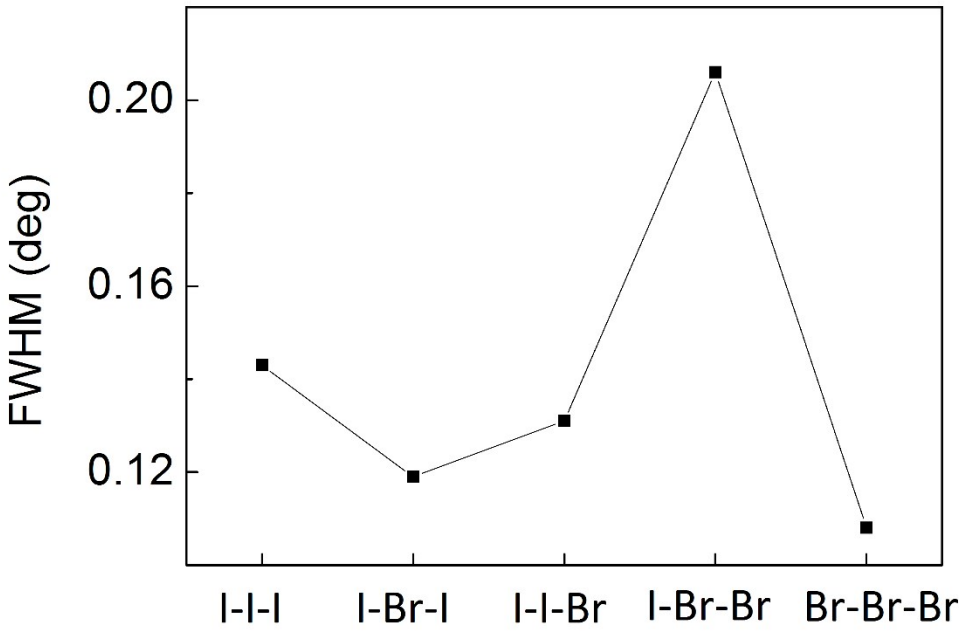

Figure S1. Full width at half maximum (FWHM) at azimuth angle of (111) in XRD for the five perovskite films.

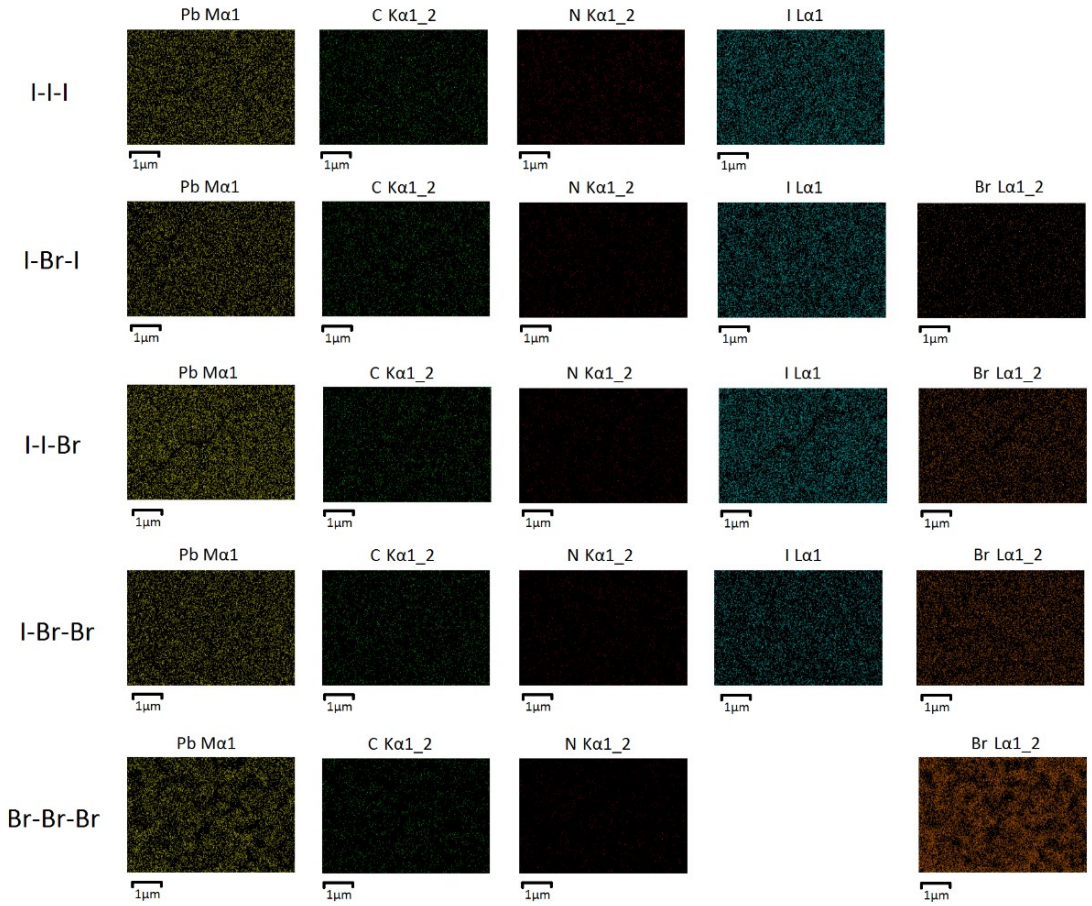

Figure S2. The EDS images of the Br element distribution for the five LDRP perovskite thin films.

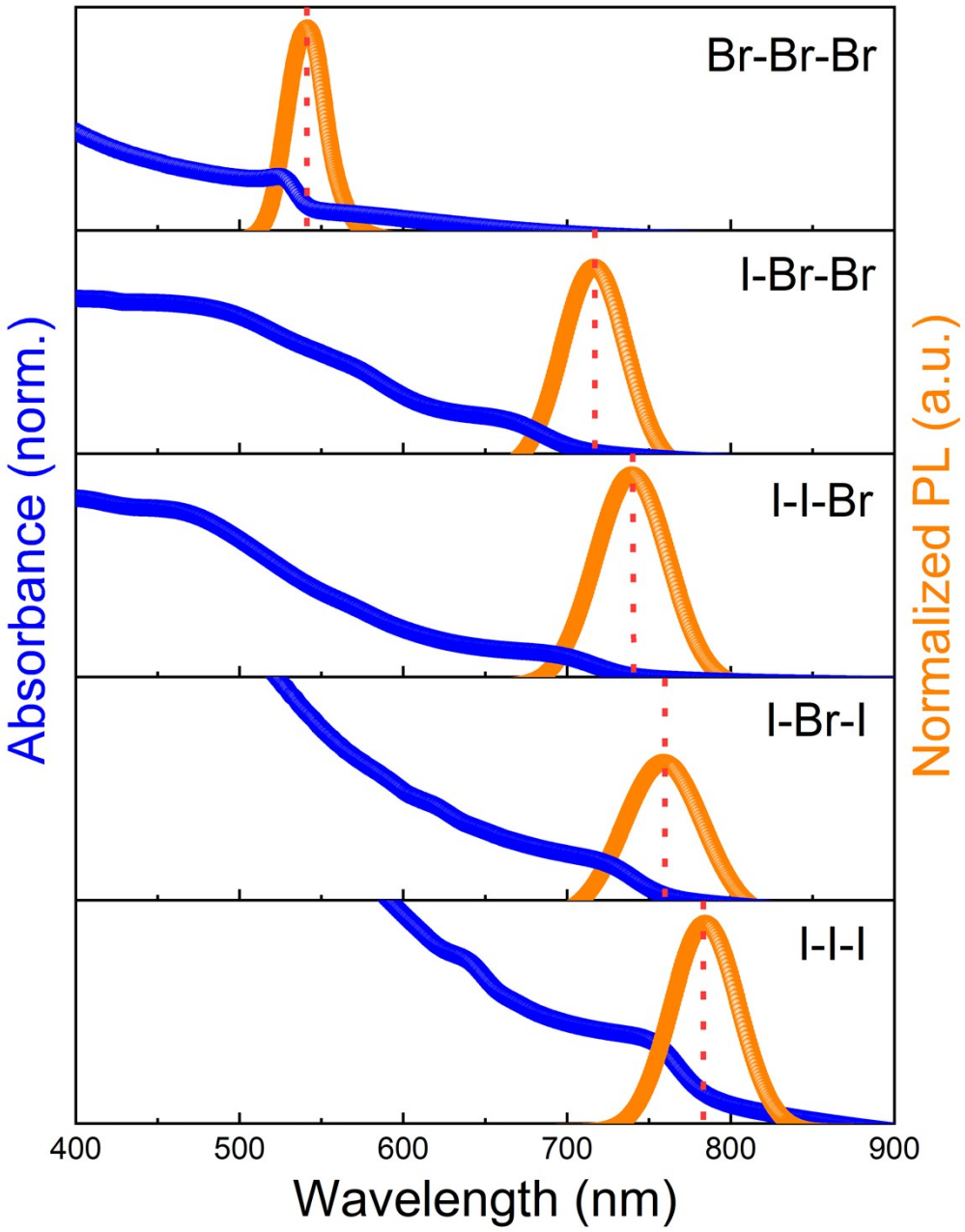

Figure S3. Normalized absorbance and PL spectra of the five LDRP perovskite films.

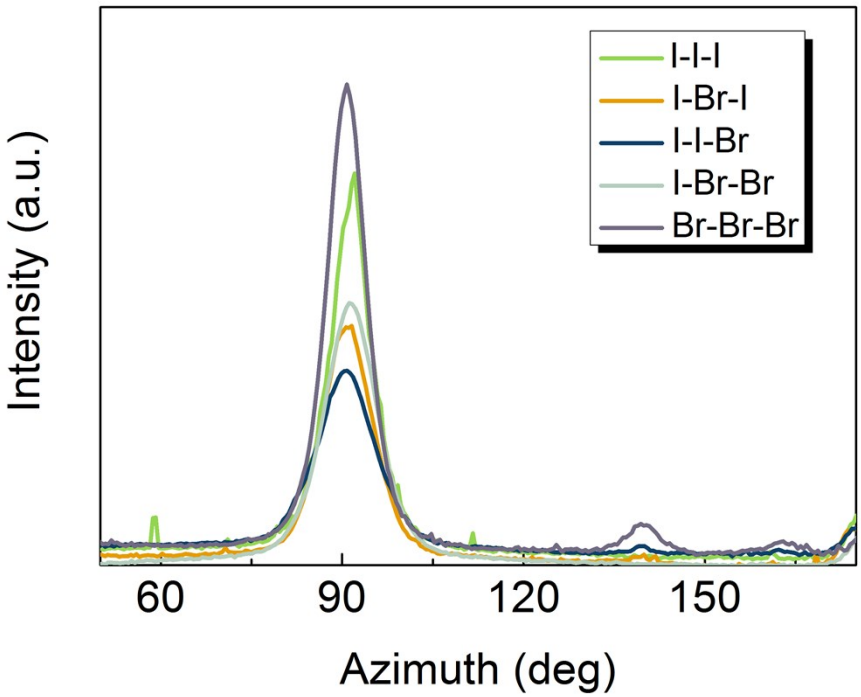

Figure S4. The pole figures showing the differences in broadness of the Azimuth angle.

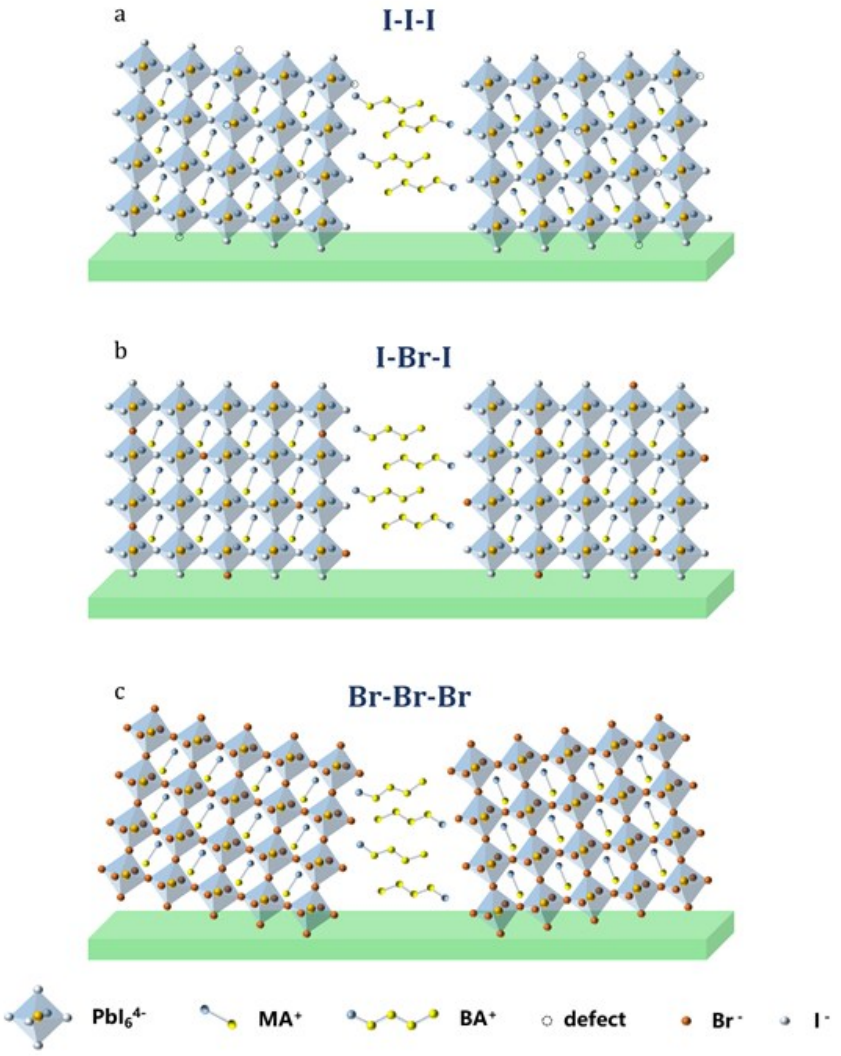

Figure S5. Schematic diagram of crystal orientation for (a) I-I-I, (b) I-Br-I and (c) Br-Br-Br perovskite films.

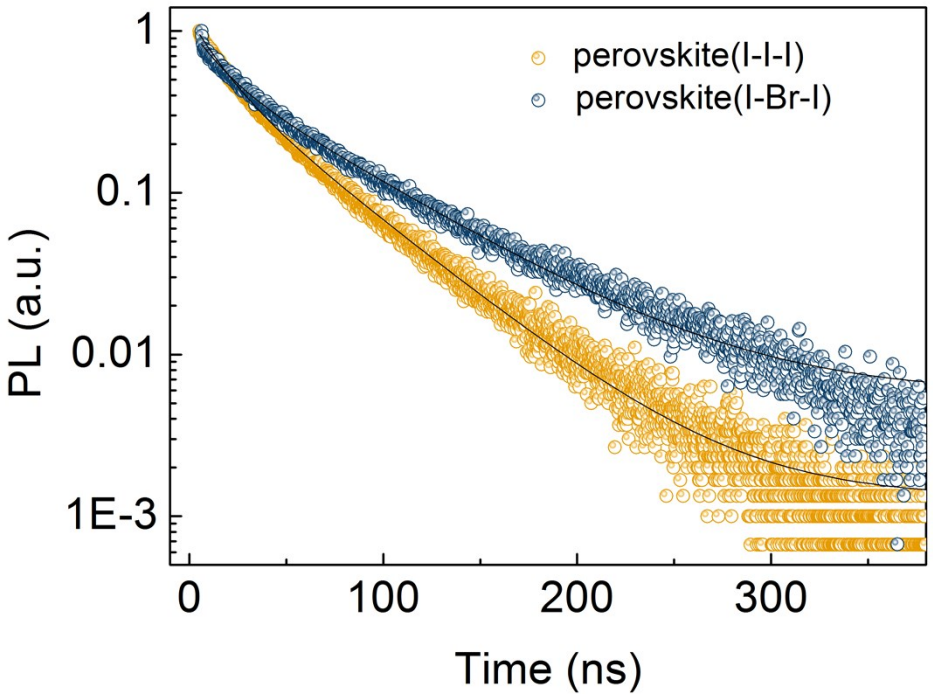

Figure S6. TRPL spectrum of the two kinds of LDRP perovskites without charge transport layers.

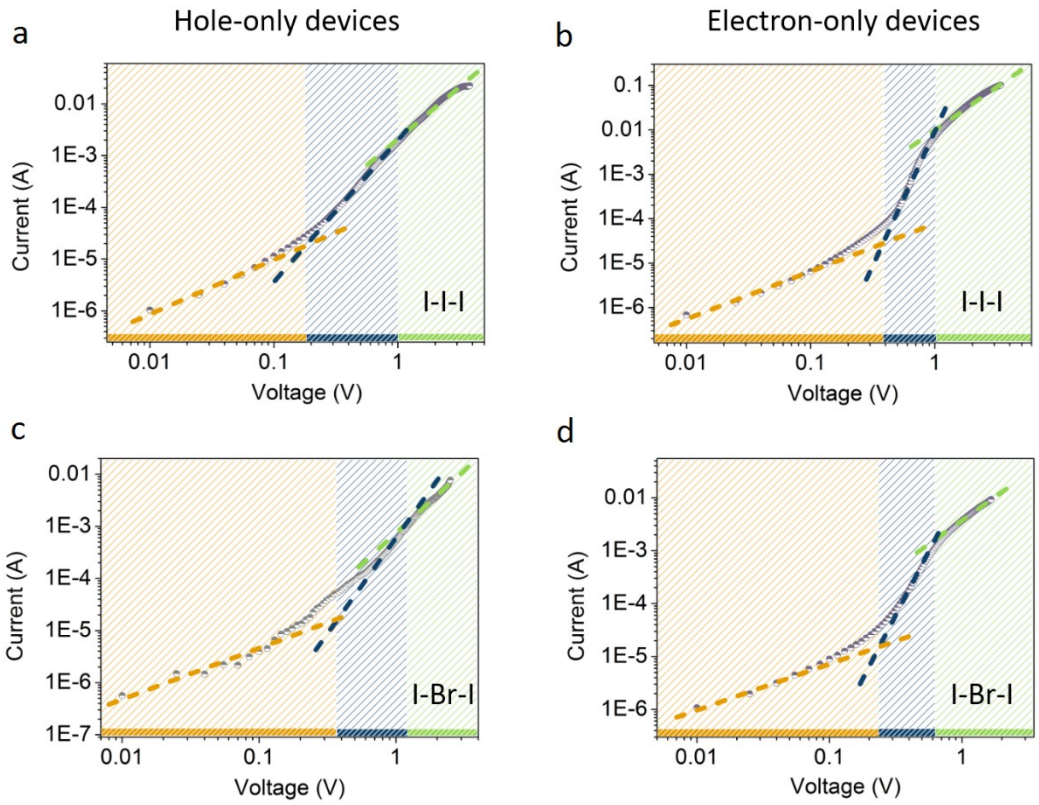

Figure S7. Dark I–V measurements of the electron-only and hole-only devices based on I-Br-I and I-I-I systems. (The orange area is the Ohmic region with a slope of 1, where the current depends on the intrinsic mobile charge carriers of the perovskites; the blue area represents the trap-filled restricted region with a slope of >2, where the current depends on the trap filling process; the green region indicates the SCLC region with a slope of 2, where the current depends on charge carrier mobility.)

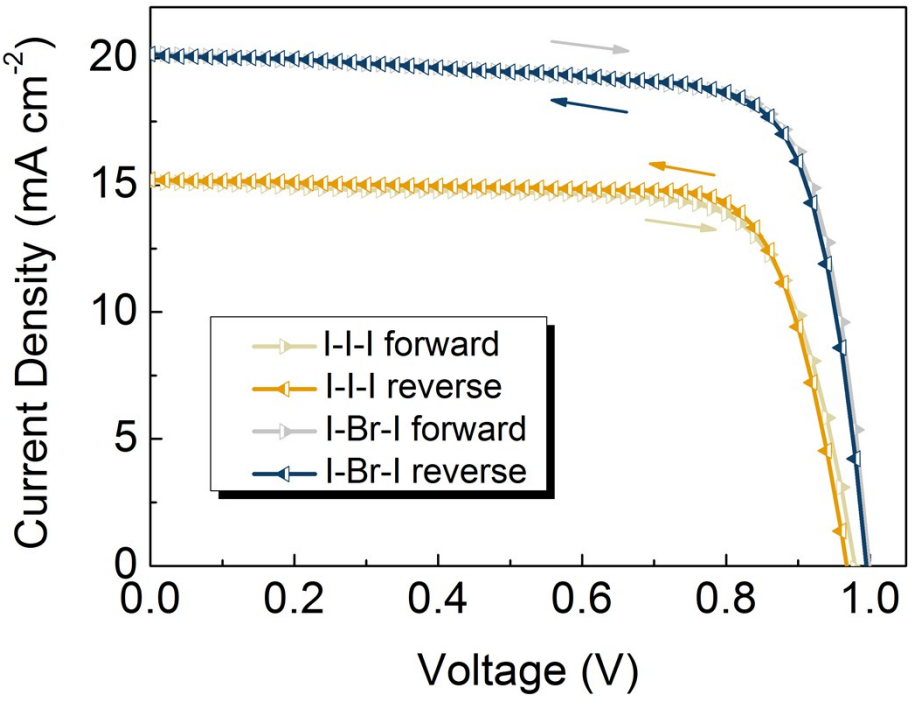

Figure S8. J–V curves of the devices with forward and reverse voltage scanning.

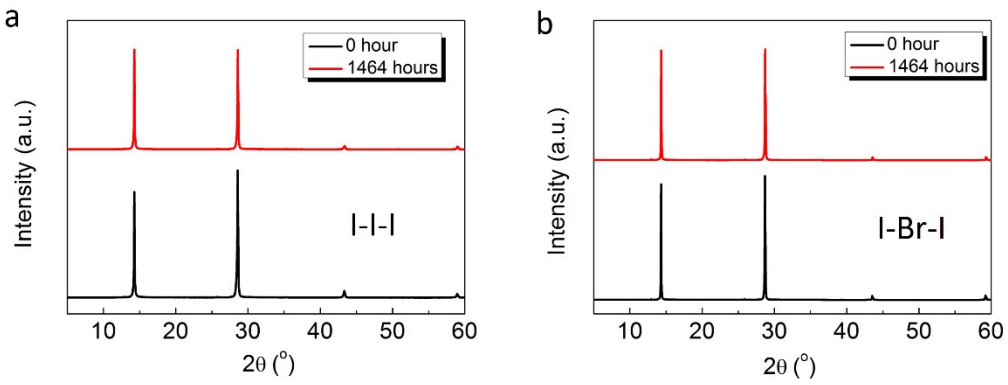

Figure S9. The XRD patterns of the (a) I-I-I and (b) I-Br-I LDRP perovskite thin films exposing in air with humidity of 55%.

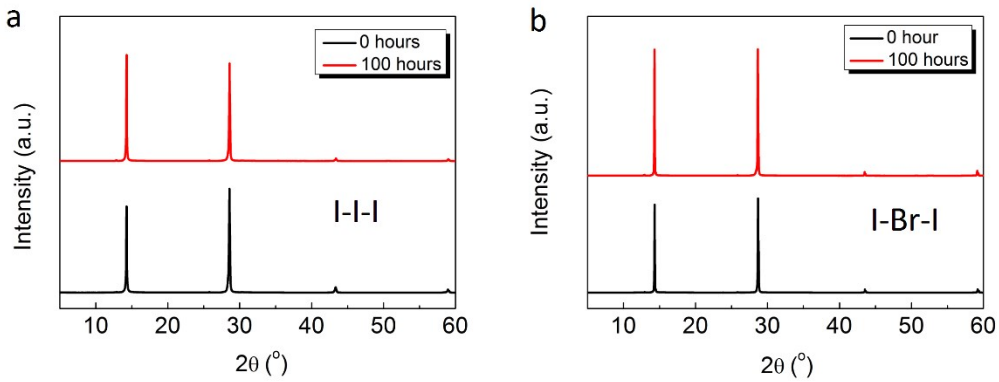

Figure S10. The XRD patterns of the (a) I-I-I and (b) I-Br-I LDRP perovskite thin films heated at 85 °C in glove box.

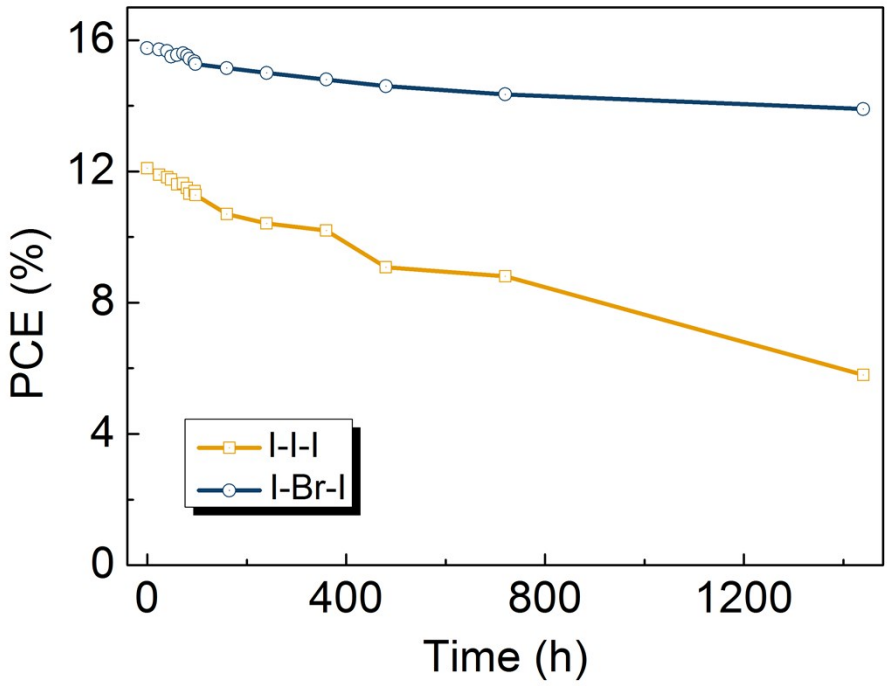

Figure S11. The variations of PCE for I-I-I and I-Br-I LDRP PSCs. The devices are stored in glove box without encapsulation.

Table S1. FWHM of (111) peak of the five LDRP perovskite films.

LDRP perovskite films	Peak position (111)	FWHM (111)
I-I-I	14.19°	0.143
I-Br-I	14.24°	0.119
I-I-Br	14.29°	0.131
I-Br-Br	14.36°	0.206
Br-Br-Br	14.94°	0.108

Table S2. Parameters of the five LDRP perovskite films from EDS.

LDRP perovskite films	Composition	Ratio (I : Br)
I-I-I	I_{16}	100% (I)
I-Br-I	$I_{14}Br_2$	7.096
I-I-Br	$I_{12}Br_4$	3.121
I-Br-Br	$I_{10}Br_6$	1.491
Br-Br-Br	Br_{16}	100% (Br)

Table S3. The carriers lifetime ($\tau_{perovskite}$, $\tau_{heterojunction}$), charge transfer time (τ_{CT}), and the carrier extraction efficiency (η) of the I-I-I and I-Br-I systems.

		I-I-I	I-Br-I
Perovskite	$\tau_{perovskite}$	31.73 ns	43.10 ns
PEDOT:PSS/perovskite	$T_{heterojunction}$	6.29 ns	2.364 ns
	τ_{CT}	7.85 ns	2.51 ns
	η	80.13%	94.18%
Perovskite/PCBM	$T_{heterojunction}$	4.013 ns	2.10 ns
	τ_{CT}	4.425 ns	2.25 ns
	η	90.69%	93.33%

Table S4. The trap-state density and charge mobility of the LDRP perovskite films.

LDRP perovskite films	$N_t(cm^{-3})$	$\mu_{electron}(cm^2\ V^{-1}\ s^{-1})$	$\mu_{hole}(cm^2\ V^{-1}\ s^{-1})$
I-I-I	2.02×10^{16}	3.68×10^{-5}	8.55×10^{-6}
I-Br-I	6.50×10^{15}	3.62×10^{-4}	1.05×10^{-5}

Table S5. Comparison between our device and literature reported BA based 2D

perovskite devices with the same n value (n=5)

Active layer	Device structures	V_{OC} [V]	J_{SC} [mA cm^{-2}]	FF [%]	PCE [%]	Perovskite film fabrication	Refs.
$BA_2MA_4Pb_5I_{16}$	ITO/SnO_2/perovskite/Spiro-OMeTAD/MoO_3/Au	1.23	17.42	67.18	14.39	in Air	1
$BA_2MA_4Pb_5I_{16}$	ITO/PEDOT:PSS/ perovskite/PCBM/Al	0.99	15.50	65.59	10.00	in Glovebox	2
$BA_2MA_4Pb_5I_{16}$	ITO/PEDOT:PSS/ perovskite/PCBM/BCP/Cu	1.05	18.35	74.93	14.40	in Glovebox	3
$(BA)_2(MA_{0.8}FA_{0.15}Cs_{0.05})_4Pb_5I_{16}$	ITO/PTAA/perovskite /C_{60}/BCP/Ag	1.12	21.38	75.32	18.04	in Glovebox	4
$(BA,GA)_2(MA)_4Pb_5I_{16}$	ITO/HTL/perovskite /PCBM/BCP/Ag	1.17	16.90	81.00	15.86	in Glovebox	5
GA-$(BA)_2(MA)_4Pb_5I_{16}$	ITO/PEDOT:PSS/ perovskite/PCBM/BCP/Ag	1.13	18.63	77.00	16.26	in Glovebox	6
$BA_2MA_4Pb_5Br_2I_{14}$	ITO/PEDOT:PSS/ perovskite/PCBM/LiF/Al	1.01	20.44	76.63	15.77	in Air	This work

References

1. C. Liang, H. Gu, Y. Xia, Z. Wang, X. Liu, J. Xia, S. Zuo, Y. Hu, X. Gao, W. Hui, L. Chao, T. Niu, M. Fang, H. Lu, H. Dong, H. Yu, S. Chen, X. Ran, L. Song, B. Li, J. Zhang, Y. Peng, G. Shao, J. Wang, Y. Chen, G. Xing and W. Huang, *Nat. Energy*, 2020, **6**, 38-45.

2. C. M. M. Soe, W. Nie, C. C. Stoumpos, H. Tsai, J.-C. Blancon, F. Liu, J. Even, T. J. Marks, A. D. Mohite and M. G. Kanatzidis, *Adv. Energy Mater.*, 2018, **8**, 1700979.

3. X. Li, G. Wu, M. Wang, B. Yu, J. Zhou, B. Wang, X. Zhang, H. Xia, S. Yue, K. Wang, C. Zhang, J. Zhang, H. Zhou and Y. Zhang, *Adv. Energy Mater.*, 2020, **10**, 2001832.

4. J. Wang, S. Luo, Y. Lin, Y. Chen, Y. Deng, Z. Li, K. Meng, G. Chen, T. Huang, S. Xiao, H. Huang, C. Zhou, L. Ding, J. He, J. Huang and Y. Yuan, *Nat. Commun.*, 2020, **11**, 582.

5. X. Lian, J. Chen, Y. Zhang, S. Tian, M. Qin, J. Li, T. R. Andersen, G. Wu, X. Lu and H. Chen, *J. Mater. Chem. A*, 2019, **7**, 18980-18986.

6. X. Lian, J. Chen, Y. Zhang, M. Qin, T. R. Andersen, J. Ling, G. Wu, X. Lu, D. Yang and H. Chen, *J. Mater. Chem. A*, 2019, **7**, 19423-19429.